

The Atmospheric Response to Realistic Arctic Sea Ice Anomalies in an AGCM during Winter

MICHAEL A. ALEXANDER

NOAA-CIRES Climate Diagnostics Center, Boulder, Colorado

UMA S. BHATT

International Arctic Research Center, University of Alaska, Fairbanks, Fairbanks, Alaska

JOHN E. WALSH AND MICHAEL S. TIMLIN

Department of Atmospheric Sciences, University of Illinois at Urbana-Champaign, Urbana, Illinois

JACK S. MILLER

Institute of Northern Engineering, University of Alaska, Fairbanks, Fairbanks, Alaska

JAMES D. SCOTT

NOAA-CIRES Climate Diagnostics Center, Boulder, Colorado

(Manuscript received 6 February 2003, in final form 9 July 2003)

ABSTRACT

The influence of realistic Arctic sea ice anomalies on the atmosphere during winter is investigated with version 3.6 of the Community Climate Model (CCM3.6). Model experiments are performed for the winters with the most (1982/83) and least (1995/96) Arctic ice coverage during 1979–99, when ice concentration estimates were available from satellites. The experiments consist of 50-member ensembles: using large ensembles proved critical to distinguish the signal from noise.

The local response to ice anomalies over the subpolar seas of both the Atlantic and Pacific is robust and generally shallow with large upward surface heat fluxes ($>100 \text{ W m}^{-2}$), near-surface warming, enhanced precipitation, and below-normal sea level pressure where sea ice receded, and the reverse where the ice expanded. The large-scale response to reduced (enhanced) ice extent to the east (west) of Greenland during 1982/83 resembles the negative phase of the Arctic Oscillation/North Atlantic Oscillation (AO/NAO) with a ridge over the poles and a trough at midlatitudes. The large-scale response was distinctly different in the Pacific, where ice extent anomalies in the Sea of Okhotsk generate a wave train that extends downstream over North America but the wave train response is greatly diminished when the model is driven by ice concentration rather than ice extent anomalies. Comparing the AGCM response to observations suggests that the feedback of the ice upon the atmospheric circulation is positive (negative) in the Pacific (Atlantic) sector. The magnitude of the wintertime response to ice extent anomalies is modest, on the order of 20 m at 500 mb. However, the 500-mb height anomalies roughly double in strength over much of the Arctic when forced by ice concentration anomalies. Furthermore, the NAO-like response increases linearly with the aerial extent of the Atlantic ice anomalies and thus could be quite large if the ice edge retreats as a result of global warming.

1. Introduction

Sea ice is a critical component of the climate system because it strongly influences albedo, surface turbulent heat fluxes, surface wind drag, and upper-ocean stratification. Thus, changes in Arctic sea ice strongly impact

local climate variability and could potentially alter the global climate via changes in the thermohaline circulation and the location of storm tracks.

In addition to a large seasonal cycle, Arctic sea ice exhibits variability on subseasonal to decadal and longer time scales (Walsh and Johnson 1979; Mysak and Manak 1989; Chapman and Walsh 1993; Fang and Wallace 1994; Parkinson et al. 1999; Polyakov and Johnson 2000; Serreze et al. 2000). Most studies have found that changes in sea ice concentration during winter primarily

Corresponding author address: Michael Alexander, NOAA-CIRES Climate Diagnostics Center, R/CDC1, 325 Broadway, Boulder, CO 80305-3328.
E-mail: Michael.Alexander@noaa.gov

result from surface heat flux (thermodynamic) and wind stress (dynamic) forcing of the ice by the atmosphere (e.g., Agnew 1993; Fang and Wallace 1994; Proshutinsky and Johnson 1997). In the Atlantic, strengthening of the North Atlantic Oscillation (NAO; e.g., Hurrell et al. 2003) is associated with an intensification of the Icelandic low and advection of anomalously warm (cold) air to the east (west) of Greenland. As a result, ice extent increases in the Labrador Sea and decreases in the Greenland–Iceland–Norwegian (GIN) Seas (Chapman and Walsh 1993), a pattern that exhibits both pronounced decadal variability and a long-term trend (Mysak et al. 1990; Slonosky et al. 1997; Deser et al. 2000, 2002). In the Pacific, Overland and Pease (1982) presented evidence that the path of synoptic storms influences the sea ice edge in the Bering Sea. On a basinwide scale, wind and heat flux anomalies associated with a wave train over the Pacific rim, which bears some resemblance to the “North Pacific Oscillation” (Rogers 1981), leads to anomalies of opposite sign in the Sea of Okhotsk and the Bering Sea (Cavaleri and Parkinson 1987; Fang and Wallace 1994).

One major exception to the paradigm of the atmosphere directly forcing ice variability occurs in the Greenland Sea where the East Greenland Current transports ice southward through the Fram Strait (Walsh and Chapman 1990), which can lead to large and long-lived anomalies in the North Atlantic (e.g., Dickson et al. 1988). Coherent variability in the atmosphere–ocean–ice system in the Arctic–North Atlantic has led to several hypotheses for decadal oscillations (Ikeda 1990; Mysak et al. 1990; Mysak and Venegas 1998; Ikeda et al. 2001; Goosse et al. 2002), which all require that sea ice anomalies have a pronounced impact on the atmosphere.

Some observational analyses also suggest that sea ice anomalies affect the overlying atmosphere. Deser et al. (2000) found that reductions in Greenland Sea ice cover and the associated anomalies in air–sea heat fluxes result in a northward shift of the local storm track, while Slonosky et al. (1997) found that reduced ice in the Greenland Sea during winter is associated with decreased sea level pressure (SLP) and 500-mb heights and increased surface air temperature (SAT) in the following winter. Other observational studies suggest that sea ice changes influence the atmosphere (e.g., Walsh 1983; Honda et al. 1996); however, it is difficult to establish cause and effect relationships solely from data without confirmation from model experiments.

Many AGCM simulations have been performed with both observed SSTs and sea ice extent (e.g., Gates et al. 1999; Rodwell et al. 1999), but analyses of these integrations have generally not focused on the role of varying sea ice on the atmosphere. In addition, several previous AGCM experiments have prescribed sea ice anomalies that are extreme compared to recent observations. For example, in the modeling studies of Newton (1973), Warshaw and Rapp (1973), and Royer et

al. (1990) all of the sea ice was removed from the Northern Hemisphere, while Williams et al. (1974) and Raymo et al. (1990) greatly reduced sea ice extent to represent paleoclimatic conditions. In these experiments, the reduction or elimination of sea ice led to an increase in SAT and reduced SLP over the Arctic, and a tendency for weaker midlatitude westerly winds.

Herman and Johnson (1978) were the first to examine the atmospheric circulation changes associated with the ice boundary conditions based on the present climate. In their perpetual January AGCM simulations, Arctic sea ice extent was specified to be either in a maximum or minimum state at all longitudes, an envelope of extreme ice conditions since the observed ice margin does not vary synchronously in all regions. Herman and Johnson found a significant response to the ice edge difference (maximum–minimum) in SLP, 700-mb temperature, and 300-mb heights over the Arctic and North Atlantic and Pacific Oceans. They noted that the full atmospheric response could not be explained by local thermodynamics, suggesting that dynamical processes were important for the far-field anomalies.

Murray and Simmonds (1995) and Simmonds and Budd (1991) examined the simulated atmospheric response to idealized specifications of sea ice fraction (concentration) in the Northern and Southern Hemispheres, respectively. In these perpetual winter experiments, the ice edge remained constant, but the amount of open water was set to a fixed value in each square containing ice. They found that decreasing sea ice concentrations lead to a local monotonic but nonlinear increase in SAT and a weakening of the midlatitude westerlies. Less ice also resulted in a significant decrease in the speeds and intensities of storms poleward of 45°N, but caused little change in the path of the storms. Parkinson et al. (2001) conducted AGCM experiments where the ice concentration was increased or decreased by a fixed amount in each grid square to quantify how errors in specification of ice fraction might influence the atmosphere. Changes in ice concentration influenced global SAT throughout the year but was greatest in fall and winter and in regions directly above where the ice concentration changed. In contrast to Murray and Simmonds (1995), Parkinson et al. (2001) found that SAT increased linearly as the ice concentration decreased.

Honda et al. (1999) examined the atmospheric response to maximum and minimum ice extent in the Sea of Okhotsk, where the difference between the two ice states was specified to be approximately twice as large as what has been observed. The model produced a very large response both locally, and downstream over the Bering Sea, Alaska, and North America. Wave activity diagnostics indicated that the surface heat flux anomalies associated with changes in ice extent generate a Rossby wave train. The difference between the two model experiments resembled the observed composite based on differences in ice concentration in the Sea of Okhotsk.

Recently, in a two-part study Magnusdottir et al. (2004, hereafter MDS) and Deser et al. (2004, hereafter DMSP) examined the atmospheric response to sea ice as well as SST anomalies in the North Atlantic in version 3 of the National Center for Atmospheric Research (NCAR) Community Climate Model (CCM3). The ice distributions used as boundary conditions in the CCM were derived from the observed trends during the past 40 years, although the magnitude of the anomalies was substantially amplified and the trend was treated as a perturbation that varied with the seasonal cycle but did not change from one year to the next. In the sea ice experiment, the mean wintertime response was strong and resembled the NAO, with anomalies of one sign over the Arctic and the opposite sign over the North Atlantic. However, the response was generally opposite to the observed atmospheric trend, suggesting a negative ice-to-atmosphere feedback.

While the aforementioned AGCM studies indicated that changes in sea ice influence the atmosphere, they all used somewhat idealized ice configurations, and most employed models with relatively coarse horizontal resolution ($\sim 5^\circ \times 5^\circ$). Coarse resolution influences both how the boundary conditions are specified and how the atmosphere responds to those anomalies. Most previous AGCM studies also used a limited number of model realizations. Given the modest signal-to-noise ratio of the atmospheric response to boundary forcing, having a large ensemble and/or long integrations is critical to obtaining robust results (e.g., Robertson et al. 2000; Sardeshmukh et al. 2000). Here, we use large ensembles of CCM simulations forced with observed Arctic sea ice conditions during the winter periods with maximum and minimum ice coverage to examine how realistic sea ice variability influences the atmospheric circulation [similar experiments were recently conducted by Raphael (2001) based on Southern Hemisphere ice variability]. Specific questions to be addressed include: By what dynamic and thermodynamic processes do sea ice anomalies influence the local and far-field atmospheric circulation? Does the atmospheric response differ to anomalies in ice concentration versus ice extent? Do the characteristics of the response differ in winter and summer? Here we examine the winter response; the summer response will be presented in a future paper.

2. Model experiments

a. Experiment design and boundary conditions

Given the complicated nature of ocean–ice–atmosphere interactions and the difficulty in simulating Arctic sea ice concentration and thickness in coupled models (Weatherly et al. 1998; Bitz et al. 2002), we focus on how sea ice influences the atmosphere using AGCM simulations. Boundary conditions for the simulations were derived from ice concentration values in version 1.1 of the Hadley Centre Ice Sea Surface Temperature

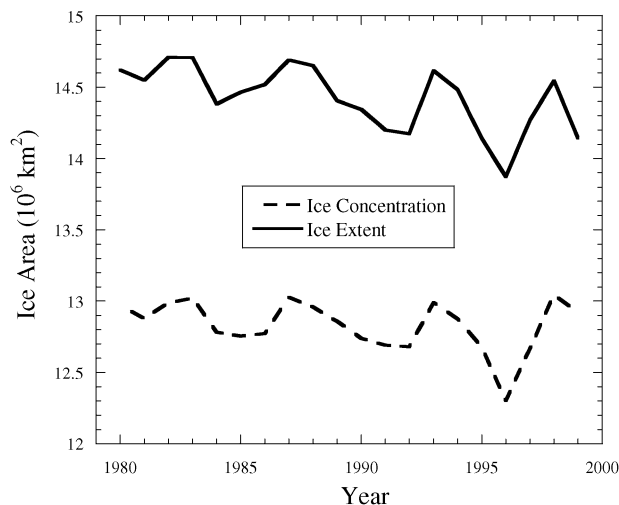


FIG. 1. The observed Arctic-wide ice cover ($\times 10^6 \text{ km}^2$) based on ice concentration and ice extent during the winter (Nov–Mar) of 1980–99 in the HadISST $1^\circ \times 1^\circ$ dataset. Ice is defined to extend over a grid square when the ice concentration exceeds 15%. The winter of 1978/79, which had extensive ice cover, was not plotted since it was unclear whether satellite data were included in the ice estimates during 1978.

dataset (HadISST; Rayner et al. 2000) during 1979–99, the period when continuous passive microwave measurements were available from satellites. Several winters (November–March) with extensive ice cover, including 1981/82, 1982/83, 1986/87, 1992/93, and 1997/98 had similar amounts of ice over the entire Arctic, while 1995/96 had substantially less ice than the other winters (Fig. 1). We focus on the winters of 1982/83 and 1995/96 because they contained large ice concentration and extent anomalies, where the anomalies evolved coherently over the course of the winter. Three model experiments have been performed in which Arctic sea ice varies according to the following observations:

- Ice extent varies over the winter of 1982/83 (Win83e),
- Ice extent varies over the winter of 1995/96 (Win96e),
- Ice concentration varies over the winter of 1995/96 (Win96c),

where the experiments are designated, in parentheses above, by the season, year and ice configuration. We also performed an extended (55 yr) control simulation in which

- Ice extent repeats the same seasonal cycle each year based on the average of the 1979–99 period (Cntle).

Implications from a similar control concentration (Cntlc) simulation are discussed at the end of section 3.

As a first step in creating the daily boundary conditions, the observed monthly mean values were interpolated to the model grid using bilinear interpolation over the open ocean and averaging of nearby grid values in coastal regions. Climatological SSTs were used ev-

erywhere ice was not present except at grid boxes adjacent to the ice where the SST was constrained not to exceed the average of -0.8°C (the lowest ice-free temperature) and the warmest SST in an adjacent grid box. In all experiments, the Arctic sea ice is specified to be 2.5 m thick; to isolate the influence of Arctic sea ice, global SSTs and sea ice in the Southern Hemisphere (specified to be 1 m thick) evolve according to the mean seasonal cycle in all of the experiments. In the extent experiments, the monthly Arctic sea ice values were specified to cover 100% of the grid square if the observed monthly averaged concentration exceeded 15%, otherwise the grid square was set to be ice free.

In order to obtain daily boundary conditions, the monthly mean ice and SST values were set to the middle of the month and then linearly interpolated in time in both the extent and concentration simulations. As a result, the transition from no ice to complete ice cover in a grid square is not instantaneous in the extent simulations, instead the amount of ice linearly increases (decreases) from 0% to 100% within the 30-day period when ice forms (melts). While this provides for a smooth transition of the ice edge in space and time, and is probably more realistic than an instantaneous transition, it also introduces fractional ice cover into the extent experiments near the ice edge.

The model boundary conditions and model response are shown on a monthly basis in Scott et al. (2003; various monthly fields from our experiments and figures relevant to the paper, which otherwise would not be shown, are presented online at <http://www.cdc.noaa.gov/~jds/Ice>). The boundary forcing for January of the Win83e experiment is shown in Fig. 2 (the boundary conditions in the Win96 experiments are shown in Fig. 14 and discussed in section 3c). Even though there are sizeable areas with less ice than normal, the winter of 1982/83 had extensive ice cover since the regions with increased ice were farther south and thus encompassed greater area in terms of square kilometers. In the Atlantic, there is more ice relative to climatology in the Labrador Sea and less in the GIN Seas, while in the Pacific there is more ice in the southern Sea of Okhotsk and in the southeastern Bering Sea and less ice on either side of the Kamchatka Peninsula. This pattern, which persists through most of the winter, closely resembles the leading EOF of sea ice over the Northern Hemisphere (Deser et al. 2000).

b. AGCM

The CCM (version 3.6), the AGCM used in this study, has 18 vertical levels and a horizontal spectral resolution of T42, approximately 2.8° latitude by 2.8° longitude when transformed to a Gaussian grid. Kiehl et al. (1998) described the model physics, while Hack et al. (1998) and Hurrell et al. (1998) examined the model's climate. Although the model has some deficiencies over the Arctic, for example, it is colder and wetter than observed

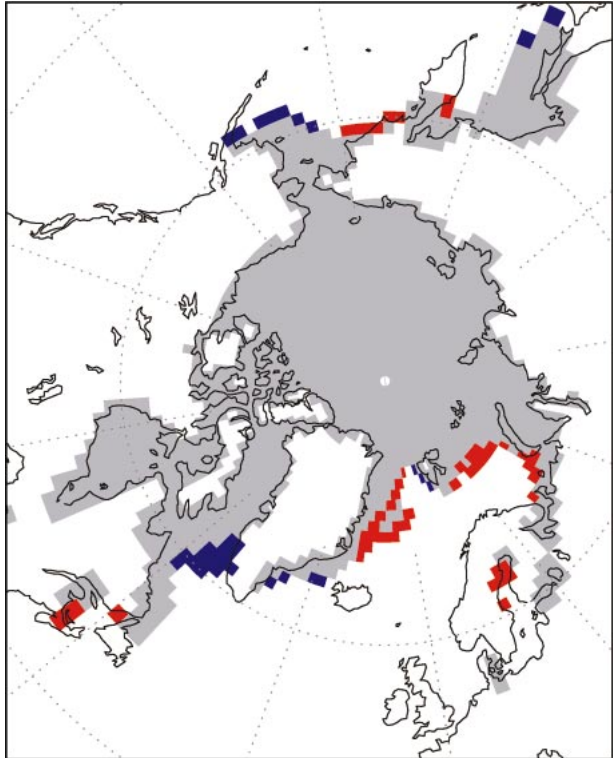


FIG. 2. Sea ice boundary conditions during Jan 1983 in the winter 1982/83 extent (Win83e) experiment. Gray indicates areas with climatological sea ice and blue (red) indicates grid squares where the ice edge has expanded (retreated) relative to climatology. Thus, the gray plus blue areas indicate the full ice extent in the Win83e experiment. Grid squares are set to be ice covered when the ice concentration exceeds 15%.

(which also occurs in most other AGCMs; Randall et al. 1998), many aspects of the earth's climate are well simulated.

c. Simulations: Initial conditions, duration, and ensemble size

The Win83e, Win95c, and Win95e experiments each consist of an ensemble of 50 CCM3 simulations that extend from October to the following April. Initializing the integrations in October allows time for the model to spinup prior to December–January–February (DJF), the period used in most of our analyses. The boundary conditions evolve identically in each simulation within the ensemble but the simulations are initialized with different atmospheric states chosen from the last 50 yr of the 55-yr Cntl integration.

We anticipate that a large ensemble is necessary because most previous AGCM experiments indicate a modest atmospheric response to realistic midlatitude SST anomalies relative to the background climate variability. The Student's t test indicates that a significant shift of the mean at the 95% confidence level requires

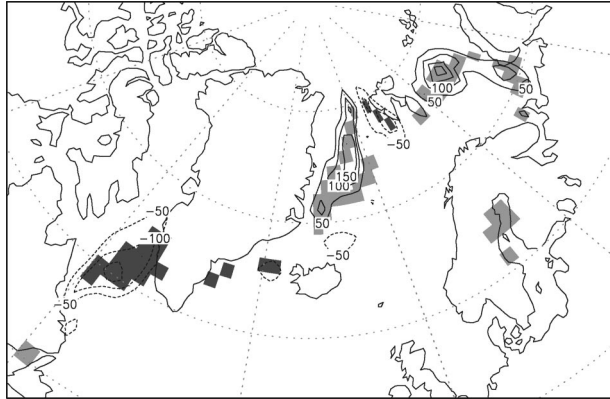


FIG. 3. Win83e net upward heat flux anomalies over the North Atlantic during DJF of 1982/83 (contours have an interval of 50 W m^{-2} ; negative values dashed, zero contour omitted). The anomalies are defined as the ensemble mean of the 50 Win83e simulations minus the long-term mean of the 55-yr control (Cntle) integration. The light (dark) shading indicates grid squares with less (more) ice in Win83e than in Cntle during Jan 1983; only one month is shown because it is unclear how to average a binary quantity like ice extent when it varies over a season.

$$N > \frac{8}{(x'/\sigma)^2}$$

(e.g., see Sardeshmukh et al. 2000), where here N is the number of simulations, x' the mean model response, and σ the standard deviation of internal atmospheric variability. Given that the winter-to-winter 500-mb height σ ranges from 40 to 60 m over much of the Arctic and Northern Hemisphere Oceans in the CCM3 control integration, a mean response of 25 m at 500 mb over DJF would require roughly 20–45 ensemble members to be significant depending on the location of the grid point.

3. Results

The anomalous atmospheric response, defined by the ensemble average of the simulations within a given experiment minus the long-term mean from the control, varies over time due to the evolution of the boundary conditions, the seasonal cycle of the climatic state, and intersample variability. In general, the anomalies are largest in December–March although for some of the experiments the pattern of the March anomalies were somewhat different than the response in the other months. Here we focus on the results in the Atlantic and Pacific sectors during DJF, the atmospheric response for all months and the DJFM average are presented in Scott et al. (2003).

a. Atlantic sector: Win83e experiment

The change in the location of the ice edge (Fig. 2) leads to intense surface heat flux anomalies in the North Atlantic sector (Fig. 3). Where the ice edge retreats, such as in the western Greenland Sea and Barents Sea,

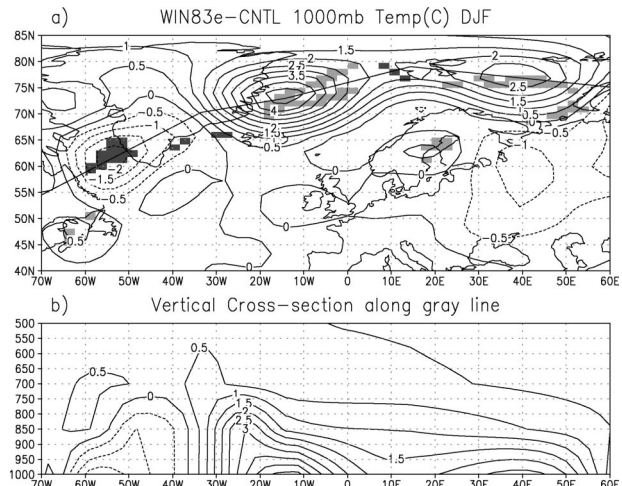


FIG. 4. Win83e temperature anomalies during DJF (a) at the 1000-mb level and (b) as a vertical cross section along the transect line shown in (a) (contours have an interval of 0.5°C ; negative contours dashed). As in Fig. 2, the light (dark) shading indicates grid squares with less (more) ice in Win83e than in Cntle during Jan 1983.

there are large net upward heat flux anomalies ($>150 \text{ W m}^{-2}$); likewise negative heat flux anomalies occur where the ice expands, including the Davis Strait and to the west of Svalbard. The flux anomalies are at much smaller spatial scale but of much larger magnitude than those associated with midlatitude SSTs. The net flux anomalies are due to the sensible, latent, and longwave fluxes, where the sensible heat flux anomalies are approximately twice (quadruple) the latent (longwave) anomalies; the solar anomalies are negligible due to the limited amount of sunlight in the Arctic during DJF.

Changes in ice extent also influence the response via frictional effects on the surface winds, because ice and water have different atmospheric drag coefficients. (The roughness length, used to compute the drag coefficient, is constant for ice but depends on wind speed and atmospheric stability over the ocean in the CCM.) From our experiments, however, it is not possible to separate the direct but likely subtle impact of changes in the surface drag on the atmospheric flow, from the circulation changes driven by the anomalous heat fluxes.

Consistent with the heat flux anomalies, the SAT anomalies (Fig. 4a) are positive above the reduced ice cover in the GIN and Barents Seas and negative over the enhanced ice cover in the Labrador Sea. The temperature response to the ice edge changes is quite shallow (Fig. 4b). In the Barents and Labrador Seas the temperature anomalies decay from $\sim 2^\circ$ at 1000 to near 0°C by 700 mb, while over the Greenland Sea the response decreases from 4° at 1000 to 0.5°C by 700 mb. The temperature anomalies extend slightly farther up into the atmosphere from 28° to 35°W over Greenland, perhaps due to interactions between the steep topography and the circulation anomalies.

The ice and temperature anomalies are nearly col-

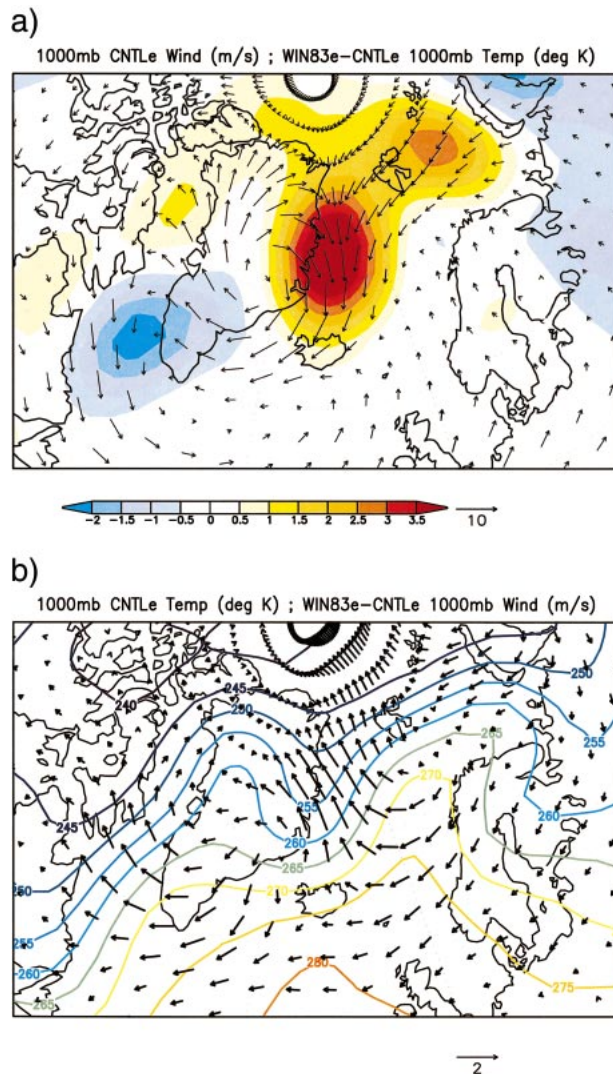


FIG. 5. The 1000-mb (a) mean vector winds from the Cntle experiment overlaid on the Win83e temperature anomalies (shaded with interval of 0.5°C) and (b) the anomalous vector winds overlaid on the mean temperature from the Cntle experiment (contoured with interval of 10.0°C). The scale vector is 10 and 2 m s^{-1} in (a) and (b), respectively.

located, indicating that advection has a modest influence on the thermal response far from the initial source of the anomalies. However, the passage of synoptic systems mixes the flux-driven thermal anomalies within a few hundred kilometers of the ice edge changes. In addition, the large-scale atmospheric response has some influence on the anomalous SAT field, through the advection of temperature anomalies by the mean circulation and by the anomalous advection across the mean temperature gradient. For example, advection by the mean flow transports the anomalously warm air from the Greenland Sea south toward Iceland and from the Barents Sea toward the east Greenland Sea (Fig. 5a). The latter leads to the surprising result of positive tem-

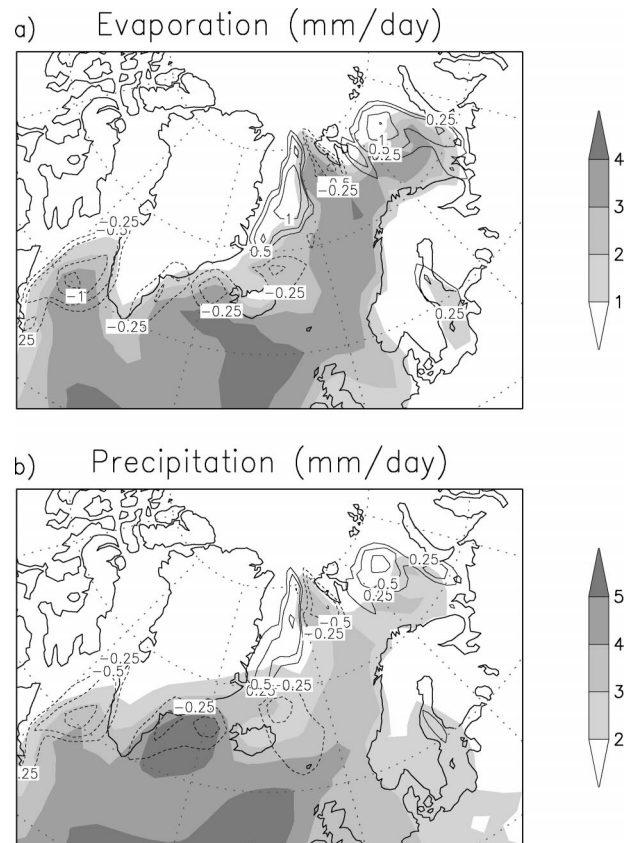


FIG. 6. Win83e (a) evaporation and (b) precipitation anomalies (contours) and the long-term mean from the Cntle simulation (shading) during DJF. The contour interval is 0.25 mm day^{-1} , where the zero line is omitted; the shading interval is 1 mm day^{-1} .

perature anomalies above increased ice cover along the west coast of Spitsbergen ($\sim 77^{\circ}\text{N}$, 10°E ; Fig. 4a). Southeasterly wind anomalies over the strong mean meridional temperature gradient in the region $65^{\circ}\text{--}80^{\circ}\text{N}$, $10^{\circ}\text{E}\text{--}30^{\circ}\text{W}$ (Fig. 5b) contribute to the anomalously warm air over the Greenland Sea seen in Fig. 4. Indeed, the magnitudes of the SAT anomalies are approximately twice as large over the Greenland Sea compared to the anomalies over the Labrador and Barents Seas, even though the magnitude of the surface flux anomalies (Fig. 3) and the latent heating associated with precipitation (Fig. 6) are of similar magnitude over the three regions.

The mean (Cntle) and anomalous (Win83e - cntle) evaporation (E) and precipitation (P) over the North Atlantic are shown in Fig. 6. Elevated values of the mean P and E (shading) coincide with the relatively warm SSTs that extend northeastward across the North Atlantic and into the GIN and Barents Seas. Both the anomalous evaporation and precipitation are located above the ice anomalies, with reduced (enhanced) P and E over the areas with more (less) sea ice. The main exception are the negative anomalies in both P and E located just to the northeast of Iceland, well removed from any ice edge changes. These reductions in P and

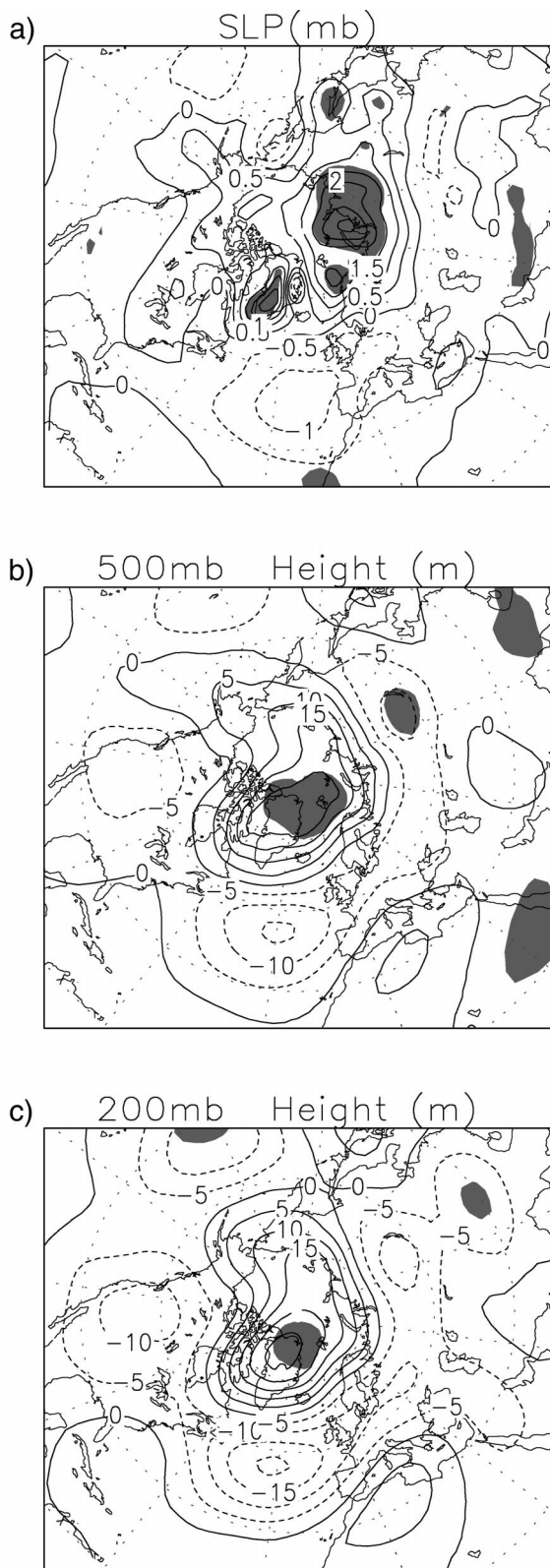


FIG. 7. Win83e response in (a) SLP, and (b) 500-, and (c) 200-mb heights during DJF. The contour interval is 0.5 mb in (a) and 5 m in (b) and (c). The shading denotes regions where the t statistic exceeds the 95% confidence level.

E coincides with reduced upward heat fluxes (Fig. 3) and the suppression of the storm track over the Iceland and Norwegian Seas in the Win83e experiment (Fig. 11a). Overall, the P and E anomalies are of similar magnitude and location and thus most ($\sim 72\%$) of the evaporation changes are compensated by similar changes in precipitation.

The change in circulation in response to the Win83e ice anomalies (Fig. 7) includes both local and large-scale features. In general, the local response is prominent near the surface with anomalously low (high) SLP above reduced (enhanced) ice extent (Fig. 7a). For example, small-scale troughs are located over the western Greenland and Bering Seas where the ice is reduced and a ridge is located over the Labrador Sea/southern Greenland and the Sea of Okhotsk, where the ice is more extensive than normal. One exception is that positive SLP anomalies are found above the reduced sea ice extent in the Barents Sea; however, this part of the response may reflect the greater influence of the large-scale changes, which include positive anomalies over most of the Arctic. The large-scale response, which is more prevalent at upper levels (Figs. 7b,c), closely resembles the negative phase of North Atlantic/Arctic Oscillation, the leading pattern of variability in the control simulation. Indeed, the pattern correlation between the response and the leading EOF of 500-mb height poleward of 20°N over the Northern Hemisphere in the Cntl simulation is 0.70. The large-scale response is equivalent barotropic, where anomalies increase in magnitude with height. The anomalies are modest with maximum amplitudes of about 15–20 m (20–25 m) at 500 mb (200 mb) and only a small portion of the response is significant at the 95% level in the middle and upper troposphere.

How sensitive is the atmospheric response to the location and extent of the ice anomalies? To address this question, we compare our results to those of MDS/DMSP who examined the CCM3 response to changes in the North Atlantic. Ice extent in MDS/DMSP's simulations, derived from the observed trends over the past 40 years, is similar to ours in that they have more ice in the Labrador Sea and less ice in the GIN and Barents Seas, but the change in aerial coverage is much greater in their experiments. In addition to an extended control run, MDS/DMSP performed two experiments based on the observed trend and approximately twice the trend.¹ The anomalous ice forcing and 500-mb response from the (a) Win83e, (b) realistic trend, and (c) exaggerated trend experiments are shown in Fig. 8. The pattern of the response is very similar in all three experiments, with positive (negative) height anomalies in high (mid)

¹ The ice extent in the realistic trend experiment is somewhat larger than the observed trend. The ice anomalies in the exaggerated ice experiment, which MDS/DMSP refer to as the ice dipole experiment, are very large—on par with the change in ice cover between winter and summer.

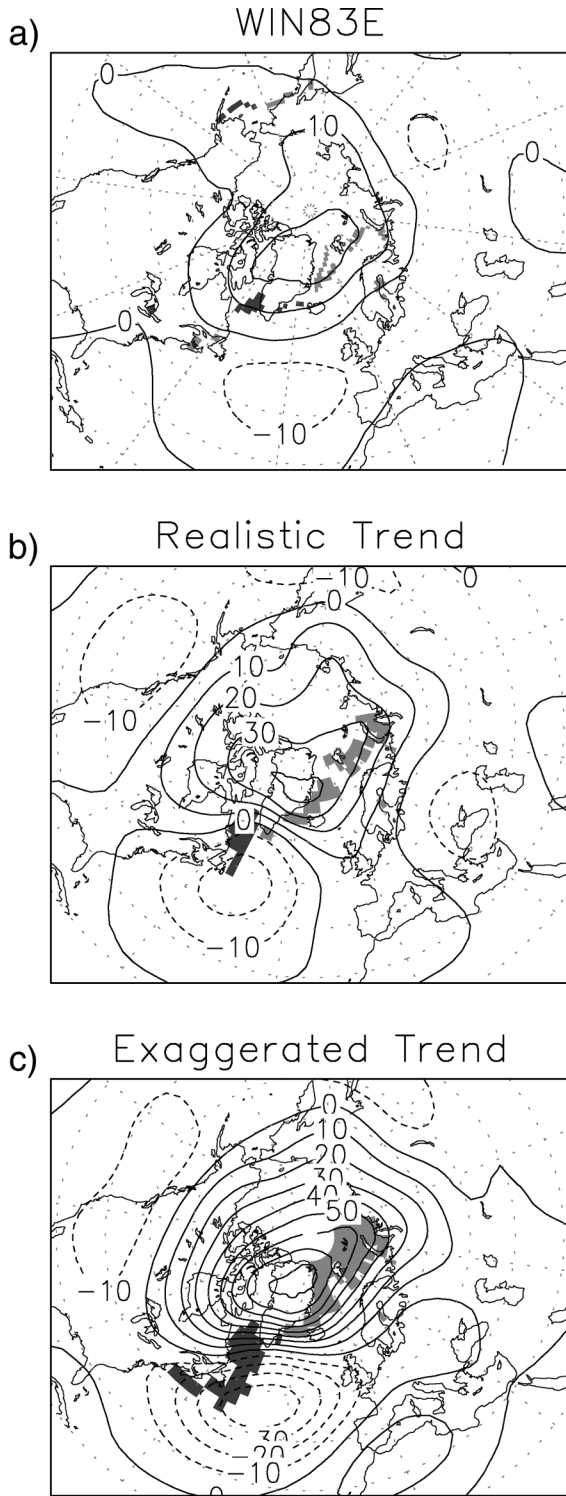


FIG. 8. The CCM response at the 500-mb level (contours) during DJF to ice anomalies (shading) in the (a) Win83e, (b) realistic trend, and (c) exaggerated trend experiments. The contour interval is 10 m, negative contours are dashed and light (dark) shading indicate regions with less (more) ice relative to the control. The latter two experiments were recently performed by MDS/DMSP, where the ice anomalies were roughly based on the observed trend and twice the trend in sea ice extent.

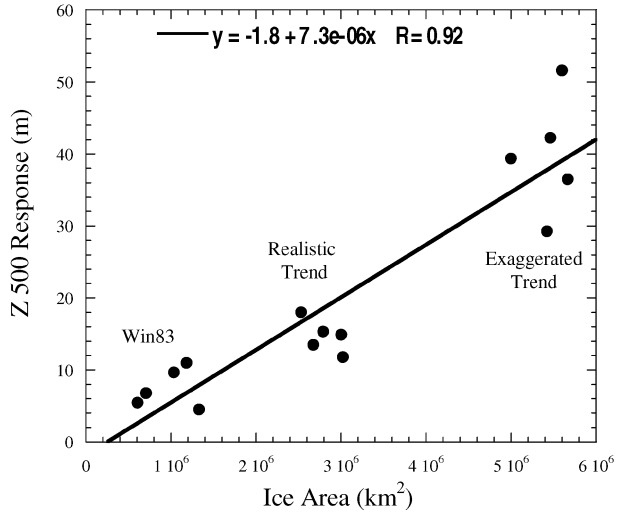


FIG. 9. Scatterplot of the magnitude of the 500-mb height anomalies vs the aerial extent of the ice anomalies averaged over the North Atlantic sector (30°–90°N, 90°–90°E) for the months of Dec–Apr in the Win83e, realistic trend, and exaggerated trend experiments. The regression line fit to the data and the correlation coefficient (R) are also shown.

latitudes, but they differ in the magnitude of the response, which increases monotonically with the extent of the ice anomalies.

The relationship between ice extent and the atmospheric response is quantified by plotting the absolute value of the monthly 500-mb anomalies versus the absolute value of the anomalous ice area, where both are averaged over the North Atlantic sector (30°–90°N, 90°–90°E). The values are presented in Fig. 9 for all three experiments for the months of December–April. The amplitude of the 500-mb response in all months is greatest in the exaggerated trend, intermediate in the realistic trend, and least in the Win83e experiment. The magnitude of the response scales nearly linearly with ice extent. In addition, the y intercept of the regression line fit to the anomalies passes within 2 m of the origin, consistent with the expectation of no response without forcing.

Comparing the simulated with observed anomalies provides some indication of how ice anomalies may be forced and/or feedback on the atmospheric circulation, with the understanding that the observed circulation anomalies result from many processes, including internal atmospheric variability and the response to SST anomalies, such as those associated with El Niño–Southern Oscillation (ENSO), in addition to the response to sea ice forcing. The atmospheric circulation pattern during the winter of 1982/83 was influenced by the very strong El Niño event in the tropical Pacific. El Niño affects sea ice in the Pacific sector via a strengthening of the Aleutian low (Niebauer 1988), as occurred in the winter of 1982/83; ENSO-induced atmospheric

1983 NCEP Reanalysis

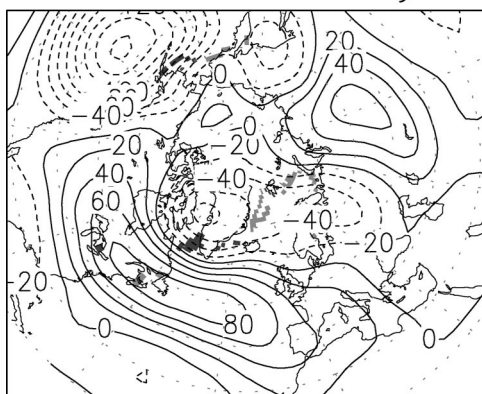


FIG. 10. Observed 500-mb height anomalies (contours) and ice anomalies (shading) during DJF of 1982/83. The contour interval is 20 m and negative contours are dashed; light (dark) shading indicates less (more) ice relative to climatology.

changes may also impact sea ice in the Atlantic sector (Gloersen 1995; Mysak et al. 1996).

The observed 500-mb height pattern during DJF of 1982/83 (Fig. 10) resembles the westward-shifted positive phase of the NAO with anomalously high (low) heights over the mid (high) latitudes. This circulation pattern, which extends to the surface (not shown), is consistent with the atmosphere forcing the ice anomalies: counterclockwise winds around the anomalous low over Greenland act to increase the ice extent in the Labrador Sea and decrease it in the GIN and Barents Seas (Deser et al. 2000, 2002). The observed 500-mb height anomaly (Fig. 10) is nearly opposite to the response of the CCM3 to the observed ice anomalies (Fig. 8b), which suggests that ice–atmosphere interactions in the North Atlantic sector damp the original atmospheric circulation anomaly, consistent with the findings of MDS/DMSP.

Deser et al. (2000) examined changes in the path of storms over the North Atlantic and GIN Seas based on observed storm counts during years with “low” and “high” values of the leading principal component of Arctic sea ice concentrations. The difference between the ice concentration in the eight low and five high winters used by Deser et al. (2000) is similar to the ice anomaly in the winter of 1982/83. We will compare the model results to the observed composite difference of these winters instead of just the winter of 1982/83 to suppress the atmospheric variability unrelated to the sea ice changes. The ice-related storm track changes in the CCM and how they compare with observations are explored by computing the bandpass-filtered near-surface meridional heat transport (1000-mb $\overline{v'T'}$ associated with 2–8-day filtered fluctuations) from both the National Centers for Environmental Prediction (NCEP) reanalysis and from the Win83 – Cntle experiments. We chose the 1000-mb level rather than 850 mb, the traditional level for computing $\overline{v'T'}$, since the temperature pertur-

bations are maximized in the boundary layer and decline rapidly with height (Fig. 4b). By this measure, the mean storm track (shading) in the CCM (Fig. 11a) and reanalysis (Fig. 11b) is centered off the east coast of North America with a northeastward extension over the GIN and Barent Seas.

The $\overline{v'T'}$ anomalies in the Win83e experiment indicate that there is a ~10%–15% reduction in strength of the simulated climatological storm track across most of the North Atlantic (Fig. 11a). Upper-level storm track diagnostics, such as the eddy kinetic energy at 200 mb, also indicate a modest suppression of storm track activity from Nova Scotia to the Norwegian Sea (Scott et al. 2003, their Fig. 2). Studies of the relationship between eddy activity and the anomalous large-scale circulation (e.g., Lau 1988; Rogers 1990; MDS) indicate that the reduction in the heart of the Atlantic storm track is consistent with a ridge over Greenland and a trough in the central North Atlantic, as found here.

The observed low–high composite indicates that the main part of the North Atlantic storm track is nearly doubled in strength when the ice is reduced in the GIN Seas (Fig. 11b); a similar result was observed during the winter of 1982/83 (Scott et al. 2003, their Fig. 1). Thus, like the height anomalies, the simulated $\overline{v'T'}$ anomalies are opposite in sign but much smaller in amplitude than the observed anomalies over the North Atlantic.

On a regional scale, the enhancement of $\overline{v'T'}$ over the southern Labrador Sea and northern Greenland Sea in the Win83e experiment (Fig. 11a) corresponds to increased low-level baroclinicity as indicated by changes in the near-surface temperature gradient (Fig. 5; Scott et al. 2003, their Fig. 3). Deser et al. found a westward shift in the observed storm track in the GIN Seas, with an increased number of storms above reduced ice cover along much of the east coast of Greenland in the low–high composite years. A similar change in the observed precipitation occurs for the low–high years and in the winter of 1983 (Scott et al. 2003, their Fig. 4). While a westward shift is also apparent in both the simulated precipitation (Fig. 6b) and $\overline{v'T'}$ (Fig. 11a), the observed low–high values (Fig. 11b) are of smaller scale and somewhat displaced relative to the model. In addition, the local change in $\overline{v'T'}$ in the CCM are collocated with a broadscale ridge, which is opposite to the relationship between the NAO and storm track found by Lau (1988) and Rogers (1990). Thus, the relationship of the anomalous near-surface eddy activity in the CCM to both the observed storm track changes and the simulated large-scale circulation anomalies is unclear from our experiments.

b. Pacific sector: Win96e and Win83e

The ice boundary conditions in the Sea of Okhotsk during the Win83e and Win96e simulations are similar to but less extensive than the somewhat idealized

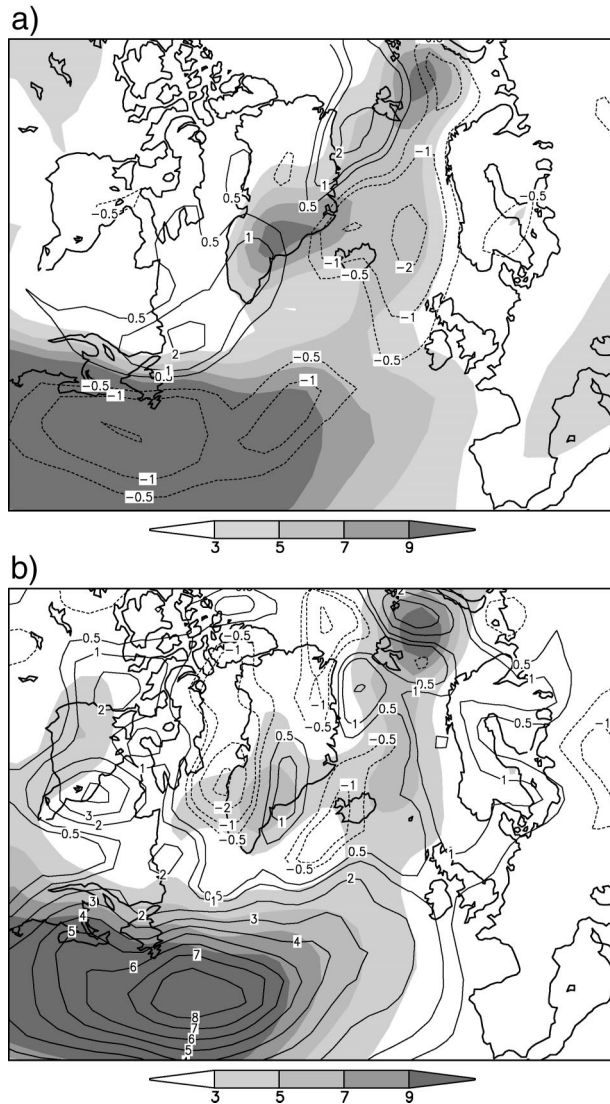


FIG. 11. The mean (shaded) and anomalous (contoured) 2–8-day bandpass-filtered meridional heat transport at 1000 mb averaged over DJF from (a) the CCM and (b) the reanalysis. Climatology is obtained from the long-term mean values in the Cntle simulation in (a) and the reanalysis in (b) over the period 1949–2000. The anomalies in (b) are based on the leading principal component of Arctic Sea ice concentration, i.e., the composite difference between years with low (1974, 1983, 1984, 1990, 1991, 1992, 1993, 1995) and high (1963, 1966, 1967, 1968, 1969) principal component values (see Deser et al. 2000). The low–high composite has more (less) ice in the Labrador (Gin and Barents) Seas, similar to those in the Win83e experiment. The anomalies in (a) are from the ensemble mean Win83e–Cntle values. The contour interval is $1 \text{ m } ^\circ\text{C s}^{-1}$, with the $+0.5$ and -0.5 contour levels included but, the 0 contour is omitted. The shading interval is $2 \text{ m } ^\circ\text{C s}^{-1}$.

“heavy” and “light” ice conditions in the AGCM experiments performed by Honda et al. (1999). The response in their AGCM experiments, obtained from the difference between the heavy and light ice simulations, consists of a large-amplitude wave train, where the magnitude of the 500-mb height anomaly centers over Kam-

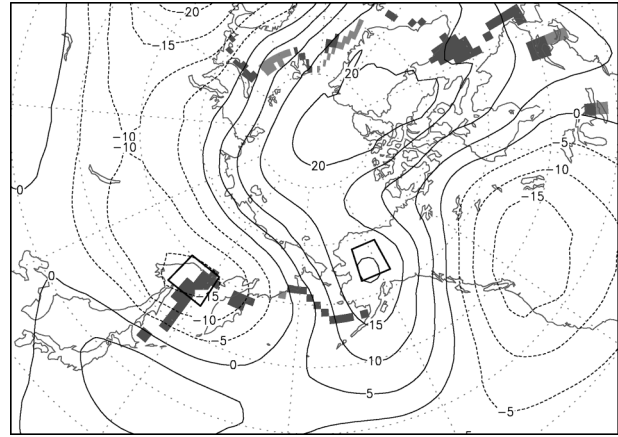


FIG. 12. The difference in 500-mb heights during DJF (contours) and ice extent during Jan (shading) between the Win83e and Win96e experiments. The contour interval is 5 m, negative contours are dashed; light (dark) shading indicates there is less (more) ice in the Win83e relative to the Win96e experiment. Boxes denote the regions used in Fig. 11.

chatka, Alaska, and Canada, exceed 150, 120, and 60 m, respectively. As a first step, we seek to confirm their findings but with more realistic ice forcing, obtained from the difference between the Win96e and Win83e experiments averaged over DJF. The pattern of the 500-mb height anomalies (Fig. 12) is similar to the wave train found by Honda et al., with a trough over eastern Siberia, a ridge over Alaska, and a trough that extends from the eastern North Pacific to central North America. However, the anomalies are only about 10%–20% as large as those in Honda et al., with the majority of the signal resulting from the forcing in the Win96e experiment (see Figs. 7b and 16c).

Several factors could contribute to the disparity between Honda et al. and our results, including differences in the boundary forcing, months used, the AGCMs employed, and the ensemble size. Honda et al. used large ice anomalies (~ 2 times the observations) but confined them to the Sea of Okhotsk. Thus, smaller ice anomalies north of Japan, and changes in the ice edge in other locations, especially in the Bering Sea, could impact the atmospheric circulation in our experiments relative to theirs. We also present the response in DJF while Honda et al. examined the response in JF but the response in our experiments is relatively unchanged if only JF was used. In addition, the AGCM used by Honda et al. is of lower horizontal resolution ($\sim 5.6^\circ \times 5.6^\circ$) but higher vertical resolution (30 levels) compared to the CCM3. Finally, the Honda et al. results are based on 5-member ensembles compared to the 50 used here. The 500-mb height differences (Win83e – Win96e) over the northern Sea of Okhotsk and Alaska (boxed areas in Fig. 12) are shown for all 50 pairs of simulations in Fig. 13. The response varies widely among the simulations, with an intraensemble standard deviation of ~ 40 m (60 m) for the center located over the Sea of Okhotsk (Alaska).

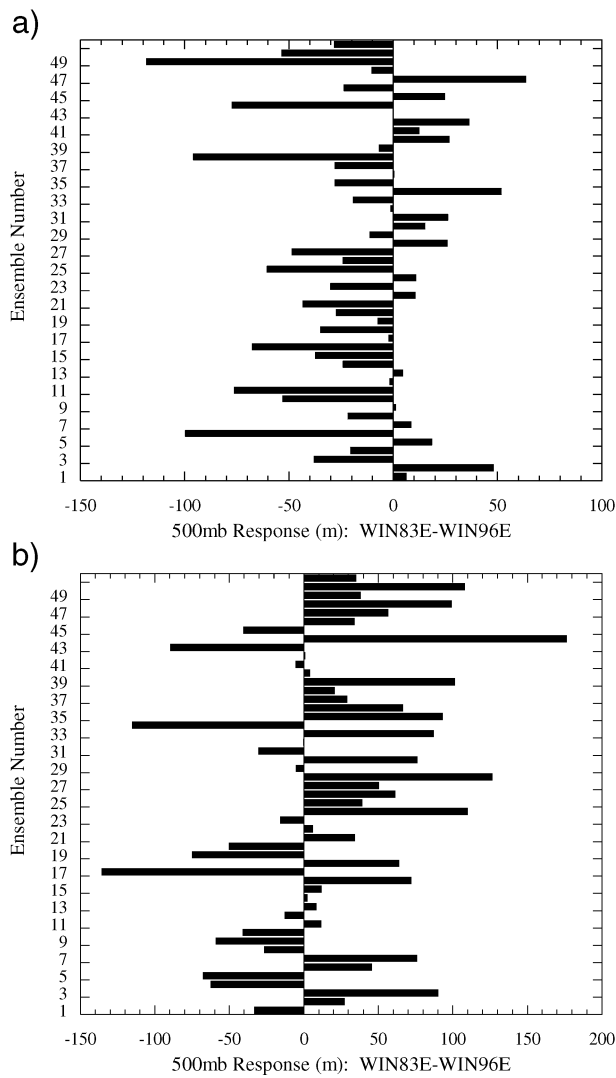


FIG. 13. The difference in the 500-mb height between the Win83e and Win96e experiments in each of the 50 ensemble members averaged over the (a) northern Sea of Okhotsk and (b) Alaskan regions shown in Fig. 12.

The variability among the ensemble members may be greater in the Alaskan center because it is farther downstream from the major source of the forcing. The importance of using a large ensemble is highlighted by comparing the 50-member ensemble average of -15 m in the Sea of Okhotsk region with 5-member sequential averages, which ranged from -33 to $+15$ m for simulations 14–18 and 30–34 as numbered in Fig. 13a.

c. The response to sea ice extent versus ice concentration

The sea ice cover in the Win96e and Win96c experiments is reduced over most of the Atlantic and Pacific sectors of the Arctic relative to the climatological ice state in the Cntle simulation (Fig. 14). Even though the

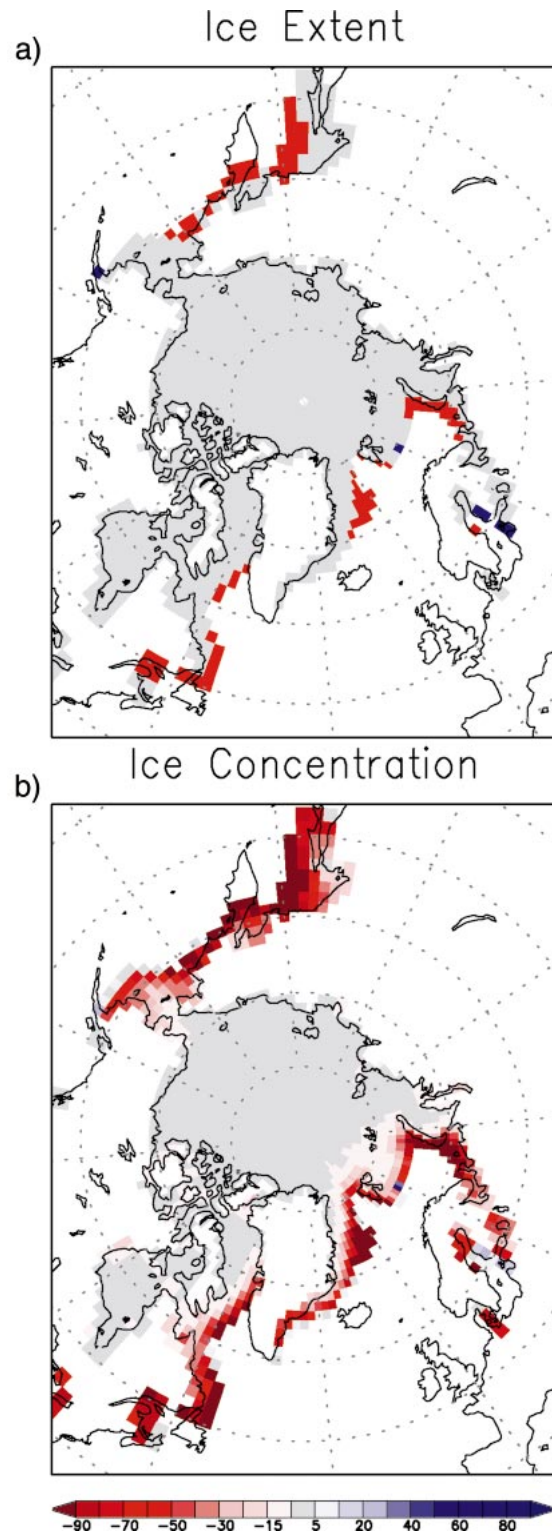


FIG. 14. Sea ice boundary conditions during Jan 1996 in the Win96 (a) extent and (b) concentration experiments. Gray indicates areas with climatological sea ice, blue (red) indicates grid squares with increased (reduced) ice relative to the climatology. The percent change in ice cover in Win96c relative to the Cntle simulation is given by the scale beneath (b).

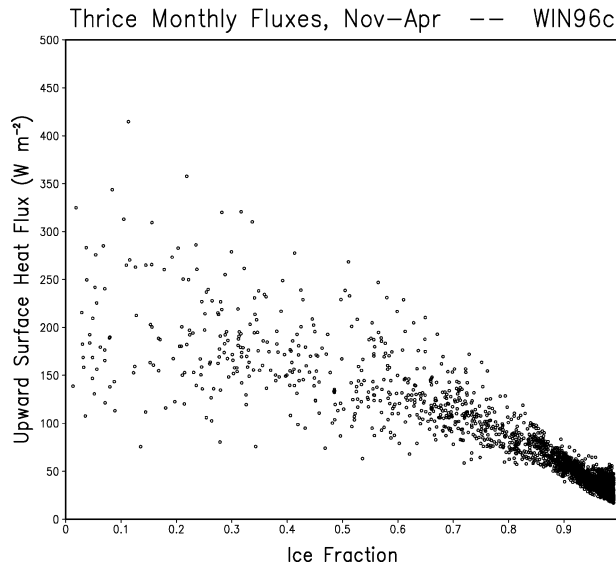


FIG. 15. Scatterplot of the ensemble average of the daily upward sensible plus latent plus longwave fluxes as a function of ice fraction at individual grid points in the Northern Hemisphere. Values are plotted on 8, 18, and 28 Nov–Apr when the ice fraction is between 1% and 99%.

marginal ice zone, the transition region between open water and full ice cover, is compact in DJF, air–sea interactions are vigorous there because surface heat fluxes are very large through leads in the ice during winter.

We examine the relationship between surface fluxes and ice fraction in a scatter diagram of the ensemble average of the daily sensible upward latent plus longwave fluxes at individual grid points as a function of ice fraction in the WIN96c experiment (Fig. 15). (Note that these are the total values and not departures from the Cntle simulation.) Since the decorrelation time scale of surface fluxes is typically less than a week, values are plotted 10 days apart in the months of November–April for all Northern Hemisphere points when the ice fraction is between 1% and 99%. In general, the fluxes increase as the ice fraction decreases from 99% toward completely ice-free conditions and this increase slows as the concentration decreases below $\sim 50\%$. However, it is difficult to estimate the response curve over the entire range of ice fraction values since the spread in the flux variability is very large at medium and low ice concentrations. Additional factors such as location, wind speed, and direction, etc., appear to have a much greater influence on the fluxes when the ice concentration is low. Taken as a whole, Fig. 15 suggests that an anomaly in the ice fraction would have a larger and more reproducible surface flux response if it occurs when the mean ice fraction is high rather than when it is low. For example, a decrease in the total sea ice concentration from 90% to 80% is likely to produce a larger–more robust flux anomaly than a decrease from 60% to 50%. Thus, relatively modest anomalies in the ice concentration along the poleward edge of the mar-

ginal ice zone during the winter of 1995/96 (Fig. 14) could lead to more intense surface flux anomalies over the northern seas and a sharper gradient across the marginal ice zone in the Win96c compared to the Win96e experiment (Scott et al. 2003, their Fig. 5).

The wintertime response to the ice extent versus ice concentration anomalies is assessed by comparing the SLP and 500-mb height anomalies during DJF from the Win96e and Win96c experiments relative to the Cntle simulation (Fig. 16). The pattern of the response in the two experiments is similar, especially at the surface. For example, in both the Win96e and Win96c experiments there are significant negative SLP anomalies over the reduced ice cover in the Sea of Okhotsk and on either side of Greenland (Fig. 14). The main difference between the experiments occurs in the free troposphere, where the 500-mb response is approximately 40%–80% larger in the concentration than in the extent simulations over the Atlantic–Asian portion of the Arctic. However, the 500-mb anomalies are not amplified outside of this area, and the aforementioned wave train emanating from the Sea of Okhotsk is diminished over North America in Win96c relative to the Win96e experiment.

The strong impact of ice concentration changes on the response may result in part to nonlinearity in the relationship between surface heat fluxes and ice fraction (which in nature would be augmented by thinning ice), where large heat fluxes can occur through small leads but then saturate as the fraction of open water increases (Ledley 1988; Simmonds and Budd 1991; our Fig. 15). One important caveat is that the atmospheric response depends on how ice extent is defined. In the extent simulations performed here, the daily ice and SSTs are linearly interpolated from their monthly means of either 0% or 100% ice cover, resulting in ice concentration values at grid points where ice formed or melted in a given month, possibly reducing the difference in the atmospheric response between the extent and concentration experiments. In addition, anomalies in both the Win96e and Win96c experiments have been defined relative to the control *extent* simulation, and thus, anomalies in the Win96c experiment include the response to the anomalous concentration and the difference in the climate between the extent and concentration simulations. To address this issue we performed a Cntlc simulation and present the Win96c – Cntlc 500-mb height during DJF in Fig. 17. While the anomalies in Win96c – Cntlc and Win96c – Cntle (Figs. 16d) differ by 10–15 m over northern North America and the North Atlantic, the broad structure of the two fields is similar and the significant anomalies over the eastern half of the Arctic are relatively unchanged. Thus, regardless of the choice of a control, our results suggest that changes in wintertime ice concentration have a more substantial impact on the large-scale atmospheric circulation than changes in ice extent alone.

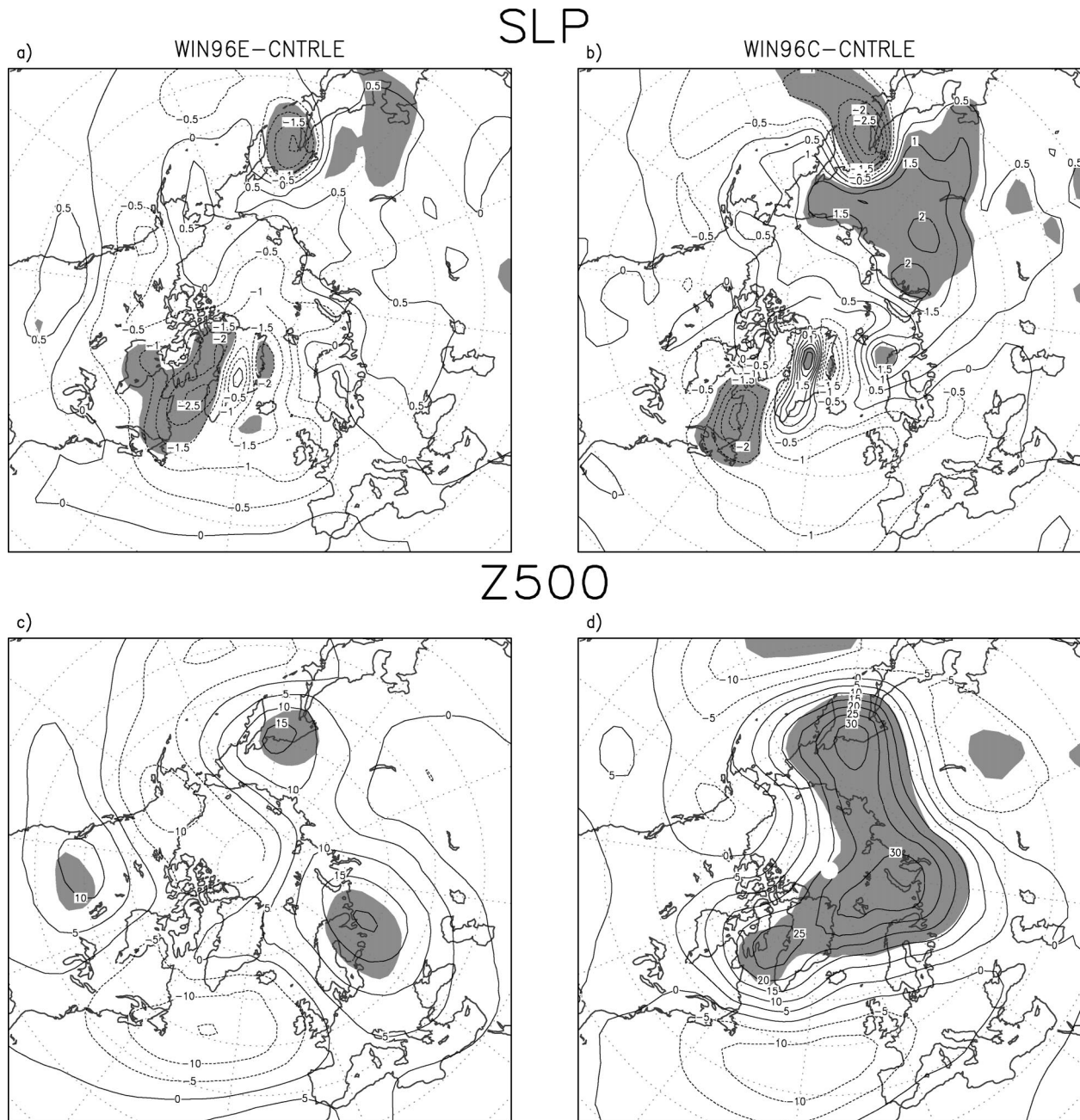


FIG. 16. The (a), (b) SLP and (c), (d) 500-mb height anomalies in the (a), (c) Win96e and (b), (a) Win96c experiments during DJF. The SLP (height) contour interval is 0.5 mb (5 m), negative contours are dashed, and shading denotes regions where the t statistic exceeds the 95% confidence level.

4. Summary and conclusions

The purpose of this study is to better understand how realistic Arctic ice anomalies influence the atmosphere during winter; the summertime response will be examined in future work. The experimental design consists of atmospheric GCM simulations in which the sea ice boundary conditions are derived from observations. Simulations are performed for 1982/83 and 1995/96, the winters with maximum and minimum ice coverage during

1979–99, when satellite estimates of sea ice were available. The experiments each consist of 50 ensemble members; using large ensembles proved critical to obtaining robust results, since the internal atmospheric variability (“climate noise”) is large in mid- and high latitudes of the CCM (see Fig. 13) and presumably in nature as well.

The sea ice departures in a given winter give rise to surface heat flux anomalies of relative small spatial scale (a few hundred kilometers) but very large amplitude

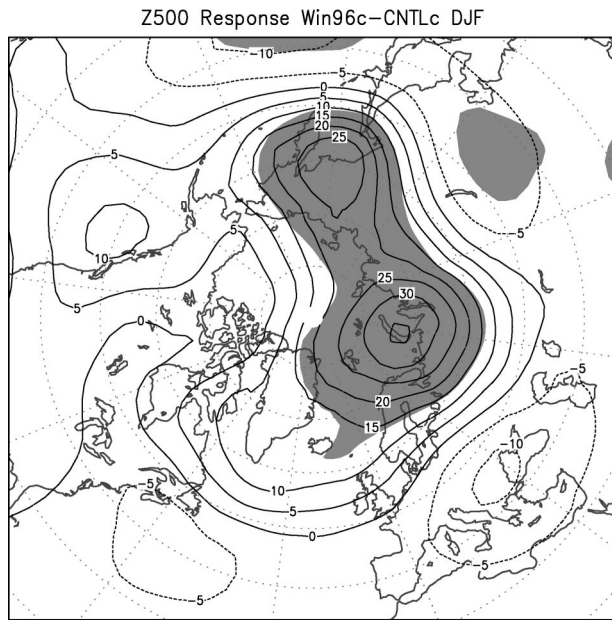


FIG. 17. The 500-mb height anomalies from the Win96c – Cntl experiments during DJF. The contour interval is 5 m, negative contours are dashed, and shading denotes regions where the t statistic exceeds the 95% confidence level.

($>100 \text{ W m}^{-2}$). The atmospheric response to this flux forcing (and perhaps to momentum forcing due to the difference in surface drag between ice and water) can be broadly separated into a local and a remote response. The local or direct response is robust but shallow, with near-surface warming, enhanced precipitation and evaporation, and below-normal sea level pressure above where the ice has receded, while the opposite occurs when the ice is more expansive. The thermal anomalies decay rapidly with height and are generally confined below 700 mb. The local response is consistent with the direct linear response to a mid- or high latitude boundary perturbation, resulting in a shallow heat source and baroclinic response: the surface low giving way to a weak ridge aloft (e.g., see Hoskins and Karoly 1981; Saravanan 1998; Peng and Whitaker 1999; Peng and Robinson 2001).

If the ice edge is collocated with the local storm track, as is the case in the Greenland Sea, then sea ice anomalies can influence the low-level baroclinicity and thereby impact the path and intensity of storms. In the Win83e experiment, the storm track shifts westward with the ice edge, resulting in enhanced (diminished) storm activity and precipitation over the west (east) Greenland Sea. While this is broadly consistent with the observational analyses of Deser et al. (2000), it was not possible to cleanly isolate the regional storm track response to sea ice anomalies from the large-scale response in our experiments.

The remote or large-scale response to changes in the ice depends on the interaction between the anomalous

surface fluxes and the large-scale circulation. The large-scale response to reduced (enhanced) ice cover to the east (west) of Greenland weakens the main branch of the North Atlantic storm track and projects strongly on the negative phase of the AO/NAO, with a ridge over the poles and a trough at midlatitudes. While these storm track and height anomalies are consistent with each other (Lau 1988; Rogers 1990; Serreze et al. 1997), it is unclear whether the storm track changes caused or resulted from the large-scale circulation changes. Peng and Robinson (2001) and Kushnir et al. (2002), however, indicate that fluctuations in the eddy-induced forcing can excite the internal modes of variability such as the AO/NAO, where interactions between the boundary-driven anomalous diabatic heating and the climatological storm track result in changes in the eddy forcing. The storm track and accompanying circulation changes can be of either sign depending on the interaction between the forcing and climatological flow; here the atmospheric response is opposite to observations, suggesting a negative ice–atmosphere feedback, which is consistent with the findings of MDS/DMSP.

Sea ice anomalies in the Pacific sector generate a direct local response with characteristics similar to those in the Atlantic sector and a large-scale wave train with centers over Siberia–Sea of Okhotsk, Alaska–Arctic Ocean, and western North America–eastern Pacific Ocean. Honda et al. (1999) found that a similar wave train developed in response to sea ice anomalies in the Sea of Okhotsk. They attributed the large-scale response, not to changes in the storm track, which is far south of the ice edge, but to excitation of stationary Rossby waves. The model response in their study and in our extent experiments does not resemble the dominant modes of internal variability over the Pacific, but bears considerable resemblance to observed composites of the circulation anomalies associated with minimum–maximum ice cover in the Sea of Okhotsk (Honda et al. 1996, 1999). Thus, unlike in the Atlantic, the Pacific ice anomalies could have a positive feedback on the atmospheric circulation. However, the wave train response was less pronounced and the AO/NAO-like response more prominent in the Win96c compared to the Win96e experiment, which suggests that the enhanced surface heat flux anomalies in the concentration simulations may preferentially excite internal modes of atmospheric variability.

Several factors influence the magnitude of the atmospheric response to the sea ice forcing, including the mean seasonal cycle of the ice–ocean–atmosphere system, the temporal and spatial evolution of the sea ice anomalies, and the presence of leads within the ice. Here, we mainly focused on the response to ice extent anomalies during DJF, where the magnitude of the response is modest: on the order of 2–2.5 mb at the surface and 15–20 m at 500 mb. The wintertime response to ice concentration anomalies, however, is twice as large as the response to the extent anomalies over the Atlantic–

Asian section of the Arctic. Additionally, a comparison of the simulations conducted here to those of MDS/DMS, indicates that the amplitude of the response to ice anomalies in the Atlantic sector scales roughly linearly with the area of the ice anomalies. Large ice anomalies, like those that could occur due to greenhouse gas emissions, had a substantial impact (>70 m at 500 mb) on the atmospheric circulation. The degree to which linear scaling applies to other ice configurations and models, as well as other seasons, requires further study.

Acknowledgments. We thank Clara Deser, Gudrun Magnusdottir, and R. Saravanan for providing us the output from their model simulations and their suggestions on improving the manuscript. We also thank Hisashi Nakamura and an anonymous reviewer for their comments and Steve Worley at NCAR for providing the HadISST dataset. This research was supported by a grant from the NOAA's Arctic Research Office issued through the International Arctic Research Center (IARC). USB was supported by the Frontier Research System for Global change through IARC. We thank NCAR for providing the CCM3 and computer support. The model simulations were performed at the Arctic Region Supercomputer Center.

REFERENCES

- Agnew, T., 1993: Simultaneous winter sea-ice and atmospheric circulation anomaly patterns. *Atmos.–Ocean*, **31**, 259–280.
- Bitz, C., J. C. Fyfe, and G. M. Flato, 2002: Sea ice response to wind forcing from AMIP models. *J. Climate*, **15**, 522–536.
- Cavaleri, D. J., and C. L. Parkinson, 1987: On the relationship between atmospheric circulation and fluctuations in sea ice extents of the Bering and Okhotsk Seas. *J. Geophys. Res.*, **92**, 7141–7162.
- Chapman, W. L., and J. E. Walsh, 1993: Recent variations of sea ice and air temperature in high latitudes. *Bull. Amer. Meteor. Soc.*, **74**, 33–47.
- Deser, C., J. E. Walsh, and M. S. Timlin, 2000: Arctic sea ice variability in the context of recent atmospheric circulation trends. *J. Climate*, **13**, 617–633.
- , M. Holland, G. Reverdin, and M. Timlin, 2002: Decadal variations in Labrador Sea ice cover and North Atlantic sea surface temperatures. *J. Geophys. Res.*, **107**, 3035, doi:10.1029/2000JC000683.
- , G. Magnusdottir, R. Saravanan, and A. Phillips, 2004: The effects of North Atlantic SST and sea ice anomalies on the winter circulation in CCM3. Part II: Direct and indirect components of the response. *J. Climate*, **17**, 877–889.
- Dickson, R. R., J. Meincke, S. A. Malmberg, and A. J. Lee, 1988: The “great salinity anomaly” in the northern North Atlantic 1968–1982. *Progress in Oceanography*, Vol. 20, Pergamon, 103–151.
- Fang, Z., and J. M. Wallace, 1994: Arctic sea ice variability on a timescale of weeks: Its relation to atmospheric forcing. *J. Climate*, **7**, 1897–1913.
- Gates, L. W., and Coauthors, 1999: An overview of the results of the Atmospheric Model Inter-comparison Project (AMIP I). *Bull. Amer. Meteor. Soc.*, **80**, 29–55.
- Gloersen, P., 1995: Modulation of sea ice cover by ENSO events. *Nature*, **373**, 503–506.
- Goosse, H., F. M. Selten, R. J. Haarsma, and J. D. Opsteegh, 2002: A mechanism of decadal variability of the sea-ice volume in the Northern Hemisphere. *Climate Dyn.*, **19**, 61–83.
- Hack, J. J., J. T. Kiehl, and J. W. Hurrell, 1998: The hydrologic and thermodynamic characteristics of the NCAR CCM3. *J. Climate*, **11**, 1151–1178.
- Herman, G. T., and W. T. Johnson, 1978: The sensitivity of the general circulation of Arctic sea ice boundaries: A numerical experiment. *Mon. Wea. Rev.*, **106**, 1649–1664.
- Honda, M., K. Yamazaki, Y. Tachibana, and K. Takeuchi, 1996: Influence of Okhotsk Sea ice extent on the atmospheric circulation. *Geophys. Res. Lett.*, **23**, 3595–3598.
- , —, H. Nakamura, and K. Takeuchi, 1999: Dynamic and thermodynamic characteristics of the atmospheric response to anomalous sea-ice extent in the Sea of Okhotsk. *J. Climate*, **12**, 3347–3358.
- Hoskins, B. J., and D. J. Karoly, 1981: The steady linear response of a spherical atmosphere to thermal and orographic forcing. *J. Atmos. Sci.*, **38**, 1179–1196.
- Hurrell, J. W., J. J. Hack, B. A. Boville, D. L. Williamson, and P. J. Rasch, 1998: The dynamical simulation of the NCAR Community Climate Model version 3. *J. Climate*, **11**, 1207–1236.
- , Y. Kushnir, G. Ottersen, and M. Visbeck, Eds., 2003: *The North Atlantic Oscillation: Climate Significance and Environmental Impact*. Geophysical Monograph Series, Vol. 134, Amer. Geophys. Union, 279 pp.
- Ikedo, M., 1990: Decadal oscillations of the air–ice–ocean system in the Northern Hemisphere. *Atmos.–Ocean*, **28**, 106–139.
- , J. Wang, and J.-P. Zhao, 2001: Hypersensitive decadal oscillations in the Arctic/subarctic climate. *Geophys. Res. Lett.*, **28**, 1275–1278.
- Kiehl, J. T., J. J. Hack, G. B. Bonan, B. A. Boville, and P. J. Rasch, 1998: The National Center for Atmospheric Research Community Climate Model: CCM3. *J. Climate*, **11**, 1131–1149.
- Kushnir, Y., W. A. Robinson, I. Bladé, N. M. J. Hall, S. Peng, and R. Sutton, 2002: Atmospheric response to extratropical SST anomalies: Synthesis and evaluation. *J. Climate*, **15**, 2205–2231.
- Lau, N. C., 1988: Variability of the observed midlatitude storm tracks in relation to low-frequency changes in the circulation pattern. *J. Atmos. Sci.*, **45**, 2718–2743.
- Ledley, T. S., 1988: For a lead-temperature feedback in climate variation. *Geophys. Res. Lett.*, **15**, 36–39.
- Magnusdottir, G., C. Deser, and R. Saravanan, 2004: The effects of North Atlantic SST and sea ice anomalies on the winter circulation in CCM3. Part I: Main features and storm track characteristics of the response. *J. Climate*, **17**, 857–876.
- Murray, R. J., and I. Simmonds, 1995: Responses of climate and cyclones to reductions in Arctic sea ice. *J. Geophys. Res.*, **100**, 4791–4806.
- Mysak, L. A., and D. K. Manak, 1989: Arctic sea ice extent and anomalies, 1953–1984. *Atmos.–Ocean*, **27**, 376–405.
- , and S. A. Venegas, 1998: Decadal climate oscillations in the Arctic: A new feedback loop for atmosphere–ice–ocean interactions. *Geophys. Res. Lett.*, **25**, 3607–3610.
- , D. K. Manak, and R. F. Marsden, 1990: Sea-ice anomalies in the Greenland and Labrador Seas during 1901–1984 and their relation to an interdecadal Arctic climate cycle. *Climate Dyn.*, **5**, 111–133.
- , R. G. Ingram, J. Wang, and A. V. D. Baaren, 1996: The anomalous sea-ice extent in Hudson Bay, Baffin Bay and the Labrador Sea during three simultaneous ENSO and NAO episodes. *Atmos.–Ocean*, **34**, 313–343.
- Newson, R. L., 1973: Response of a general circulation model of the atmosphere to the removal of the Arctic ice cap. *Nature*, **241**, 39–40.
- Niebauer, H. J., 1988: Effects of El Niño–Southern Oscillation and North Pacific weather patterns on interannual variability in the southern Bering Sea. *J. Geophys. Res.*, **93**, 5051–5068.
- Overland, J. E., and C. H. Pease, 1982: Cyclone climatology of the Bering Sea and its relation to cyclone extent. *Mon. Wea. Rev.*, **110**, 5–13.

- Parkinson, C. L., D. J. Cavalieri, P. Gloersen, H. J. Zwally, and J. Comiso, 1999: Arctic sea ice extents, areas and trends, 1978–1996. *J. Geophys. Res.*, **104**, 20 837–20 856.
- , D. Rind, R. J. Healy, and D. G. Martinson, 2001: The impact of sea ice concentration on climate model simulations with the GISS GCM. *J. Climate*, **14**, 2606–2623.
- Peng, S., and J. S. Whitaker, 1999: Mechanisms determining the atmospheric response to midlatitude SST anomalies. *J. Climate*, **12**, 1393–1408.
- , and W. A. Robinson, 2001: Relationships between atmospheric internal variability and the responses to an extratropical SST anomaly. *J. Climate*, **14**, 2943–2959.
- Polyakov, I. V., and M. A. Johnson, 2000: Arctic decadal and interdecadal variability. *Geophys. Res. Lett.*, **27**, 4097–4100.
- Proshutinsky, A. Y., and M. A. Johnson, 1997: Two circulation regimes of the wind driven Arctic Ocean. *J. Geophys. Res.*, **102**, 12 493–12 514.
- Randall, D., and Coauthors, 1998: Status of and outlook for large-scale modeling of atmosphere–ice–ocean interactions in the Arctic. *Bull. Amer. Meteor. Soc.*, **79**, 197–219.
- Raphael, M., 2001: Response of the large-scale, Southern Hemisphere extratropical atmospheric circulation to extremes of Antarctic sea-ice concentration in a general circulation model. *Polar Geogr.*, **25**, 218–238.
- Raymo, M. E., D. Rind, and W. F. Ruddiman, 1990: Climatic effects of reduced Arctic sea ice limits in the GISS II general circulation model. *Paleoceanography*, **5**, 367–382.
- Rayner, N. A., D. E. Parker, P. Frich, E. B. Horton, C. K. Folland, and L. V. Alexander, 2000: SST and sea ice fields for ERA40. *Proc. Second WCRP Int. Conf. on Reanalysis*, Reading, United Kingdom, WCRP, 18–21.
- Robertson, A. W., M. Ghil, and M. Latif, 2000: Interdecadal changes in atmospheric low-frequency variability with and without boundary forcing. *J. Atmos. Sci.*, **57**, 1132–1140.
- Rodwell, M. J., D. P. Rowell, and C. K. Folland, 1999: Oceanic forcing of the wintertime North Atlantic Oscillation and European climate. *Nature*, **398**, 320–323.
- Rogers, J. C., 1981: Spatial variability of seasonal sea-level pressure and 500 hPa height anomalies. *Mon. Wea. Rev.*, **109**, 2093–2105.
- , 1990: Patterns of low-frequency monthly sea level pressure (1899–1986) and associated cyclone frequencies. *J. Climate*, **3**, 1364–1379.
- Royer, J. F., S. Planton, and M. Deque, 1990: A sensitivity experiment for the removal of Arctic sea ice with the French spectral general circulation model. *Climate Dyn.*, **5**, 1–17.
- Saravanan, R., 1998: Atmospheric low frequency variability and its relationship to midlatitude SST variability: Studies using the NCAR Climate System Model. *J. Climate*, **11**, 1386–1404.
- Sardeshmukh, P. D., G. P. Compo, and C. Penland, 2000: Changes of probability associated with El Niño. *J. Climate*, **13**, 4268–4286.
- Scott, J. D., M. A. Alexander, M. S. Timlin, U. S. Bhatt, J. Miller, and J. E. Walsh, cited 2003: CCM3 sea ice forcing experiments: Boundary conditions and response in winter. [Available online at <http://www.cdc.noaa.gov/~jds/Ice/>]
- Serreze, M. C., F. Carse, R. G. Barry, and J. C. Rogers, 1997: Icelandic low cyclone activity: Climatological features, linkages with the NAO, and relationships with recent changes in the Northern Hemisphere circulation. *J. Climate*, **10**, 453–464.
- , and Coauthors, 2000: Observational evidence of recent change in the northern high-latitude environment. *Climatic Change*, **46**, 159–207.
- Simmonds, I., and W. F. Budd, 1991: Sensitivity of the Southern Hemisphere circulation to leads in the Antarctic pack ice. *Quart. J. Roy. Meteor. Soc.*, **117**, 1003–1024.
- Slonosky, V. C., L. A. Mysak, and J. Derome, 1997: Linking Arctic sea ice and atmospheric circulation anomalies on interannual and decadal timescales. *Atmos.–Ocean*, **35**, 333–366.
- Walsh, J. E., 1983: Role of sea ice in climate variability: Theories and evidence. *Atmos.–Ocean*, **21**, 229–242.
- , and C. M. Johnson, 1979: An analysis of Arctic sea ice fluctuations, 1953–77. *J. Phys. Oceanogr.*, **9**, 580–591.
- , and W. L. Chapman, 1990: Arctic contribution to upper-ocean variability in the North Atlantic. *J. Climate*, **3**, 1462–1473.
- Warshaw, M., and R. R. Rapp, 1973: An experiment on the sensitivity of a global acidulation model. *J. Appl. Meteor.*, **12**, 43–49.
- Weatherly, J. W., B. P. Briegleb, W. G. Large, and J. A. Maslanik, 1998: Sea ice and polar climate in the NCAR CSM. *J. Climate*, **11**, 1472–1486.
- Williams, J., R. G. Barry, and W. Washington, 1974: Simulation of the atmospheric circulation using the NCAR global circulation model with ice age boundary conditions. *J. Appl. Meteor.*, **13**, 305–317.